Lattice dynamics of the α and β phases of $LiFe_5O_8$

M. N. Iliev,[1] V. G. Ivanov,[2] N. D. Todorov,[2] V. Marinova,[3] M. V. Abrashev,[2] R. Petrova,[4] Y.-Q. Wang,[1] and A. P. Litvinchuk[1]

[1]*Texas Center for Superconductivity and Department of Physics, University of Houston, Houston, Texas 77204-5002, USA*

[2]*Faculty of Physics, University of Sofia, BG-1164 Sofia, Bulgaria*

[3]*Institute for Optical Materials and Technologies, Bulgarian Academy of Sciences, BG-1113 Sofia, Bulgaria*

[4]*Institute for Mineralogy and Crystallography, Bulgarian Academy of Sciences, BG-1113 Sofia, Bulgaria*

(Received 5 January 2011; published 27 May 2011)

The polarized Raman spectra of the inverse spinel $LiFe_5O_8$ (LFO) were studied for both B-site-ordered (α) and B-site-disordered (β) phases. The symmetry of all the Raman lines was determined and an assignment to phonon modes involving specific atomic motions was done by comparison to lattice dynamics calculations. The spectra exhibit strongly resonant behavior, the enhancement of some one-phonon bands and all the two-phonon bands being probably related to the Franck-Condon mechanism of excitation and decay of the electronic *d-d* transition of Fe^{3+}. The disordered β phase, obtained by rapid quenching after postannealing at a temperature above the nominal order-disorder transition, coexists with remnants of the α phase.

DOI: 10.1103/PhysRevB.83.174111 PACS number(s): 78.30.−j, 63.20.−e, 75.47.Lx

I. INTRODUCTION

The ferrimagnetic spinel $Li^{1+}_{0.5}Fe^{3+}_{2.5}O^{2-}_4$ or $LiFe_5O_8$ (LFO) is prospective for applications. It could be used as material for rechargeable lithium batteries and as a ferrimagnet with high Curie temperature (620 °C) it may find use in magnetic storage devices.[1,2] $LiFe_5O_8$ also attracts attention due to the specific 1:3 ordering of Li^{1+} and Fe^{3+} at the octahedral B sites resulting in $P4_132/P4_332$ structure.[3,4] At temperatures above 720–750 °C the ordering is destroyed and Li and Fe distribute randomly over the B sites, the averaged structure becoming $Fd\bar{3}m$. The lattice dynamics of LFO is scarcely studied. Raman spectra of polycrystalline samples have been reported by Aroca *et al.*,[5] Julien *et al.*,[6] and Cook and Manley.[7] They are consistent with respect to the Raman line frequencies in the ordered α phase, but no assignment to corresponding phonon modes of given symmetry and/or definite atomic motions has been made. In addition, there is some confusion concerning the reported Raman spectra of the disordered β phase. Indeed, these spectra differ significantly from one another and appear much richer than expected for the $Fd\bar{3}m$ structure. Moreover, the β-phase Raman spectrum reported in Ref. 6 strongly resembles that of α-Fe_2O_3,[8] whereas that in Ref. 7 is practically identical to the α-phase spectrum. The infrared (IR) absorption of LFO between 300 and 800 cm^{-1} has been studied by Wolska *et al.*[9] The comparison of the IR spectra of the α and β phases shows strong reduction of part of the absorption bands in the disordered phase. Nevertheless, their number remains higher than the expected only four IR phonon modes for the $Fd\bar{3}m$ structure.

II. SAMPLES AND EXPERIMENTAL

We studied two different sets of $LiFe_5O_8$ crystals, assigned as LFO-M1 and LFO-M2, obtained through the high-temperature-solution growth method in Pt crucibles using two different solvents. The solvent in the case of LFO-M1 was PbO:PbF_2:LiCl:B_2O_3, the ratio $LiFe_5O_8$:solvent being 1:7. The mixture was sealed in the crucible and maintained at temperature of 1200 °C for 48 hours and then slowly cooled at a rate of 0.5 °C/hour to 920 °C. In the case of LFO-M2 the Bi_2O_3: LiF solvent was used and the $LiFe_5O_8$:solvent mixture was melted at 1050 °C. The crystal growth was accomplished during the high-temperature-solution cooling in the interval 1050–850 °C at a rate of 0.5 °C/hour. The crystals were typically of octahedral shape, 2–3 mm in size.

The crystallographic characterization of as-grown LFO-M1 and LFO-M2 was carried out by x-ray analyses. The single-crystal data were collected at room temperature on an x-ray diffractometer (SuperNova Oxford Diffraction) with Mo radiation ($\lambda = 0.071073$ nm). The structures were solved by direct methods using SHELXL-97[10] and refined by the full matrix least-squares procedure on F2 with SHELXL-97.[11] It was confirmed that the structure of the crystals is $P4_332$ with lattice constants 8.3339 Å for LFO-M1 and 8.3292 Å for LFO-M2. The magnetic transition temperature as determined by a vibrating sample magnetometer was 892 ± 3 K for both types of crystals. A detailed description of single-crystal growth and samples characterization will be given elsewhere.[12]

The disordered β phase was obtained by postannealing of LFO-M1 crystals in air for two hours at 880 or 900 °C and rapid quenching in liquid nitrogen. The single-crystal diffraction in this case showed higher symmetry $Fd\bar{3}m$ structure with lattice constant $a = 8.3409$ Å and only one octahedral position statistically occupied by Fe and Li atoms.

The polarized Raman spectra were measured under the microscope using T64000 and LabRAM HR Raman spectrometers. The spectra were obtained from (100) or (111) crystal surfaces in backscattering configuration with 633 nm (1.96 eV), 515 nm (2.41 eV), 488 nm (2.54 eV), and 458 nm (2.71 eV) excitation. The symmetry of Raman lines was determined by their appearance or absence in XX, XY, $X'X'$, and $X'Y'$ scattering configurations from (100) surface. In this notation the first and second letters stand for the polarization of incident and scattered light, X, Y, X', and Y' being parallel to the [100], [010], [110], and [$\bar{1}$10] crystallographic directions, respectively. The notations HH and HV, used for scattering from the (111) surface, correspond

TABLE I. Wyckoff notations and irreducible representations for the nonequivalent atomic sites in the B-site ordered $P4_332$ (SG 212) and B-site disordered $Fd\bar{3}m$ (SG 227) structures of $LiFe_5O_8$ (Ref. 13). The numbering of the nonequivalent Fe and O sites in the $P4_332$ structure follows that in Ref. 4. Selection rules for the Raman-active modes at the investigated scattering configurations are also given.

$P4_332$ Ordered Phase

Atom	Wyckoff Notation	Irreducible Representantions
Li	4*b*	$A_2 + E + 2F_1 + F_2$
Fe1	12*d*	$A_1 + 2A_2 + 3E + 5F_1 + 4F_2$
Fe2	8*c*	$A_1 + A_2 + 2E + 3F_1 + 3F_2$
O1	8*c*	$A_1 + A_2 + 2E + 3F_1 + 3F_2$
O2	24*e*	$3A_1 + 3A_2 + 6E + 9F_1 + 9F_2$

Modes Classification

$$\Gamma_{\text{Raman}} = 6A_1 + 14E + 20F_2$$
$$\Gamma_{\text{IR}} = 21F_1$$
$$\Gamma_{\text{silent}} = 8A_2$$
$$\Gamma_{\text{acoustic}} = F_1$$

$Fd\bar{3}m$ Disordered Phase

Atom	Wyckoff Notation	Irreducible Representantions
Li/Fe1	16*d*	$A_{2u} + E_u + 2F_{1u} + F_{2u}$
Fe2	8*a*	$F_{1u} + F_{2g}$
O	32*e*	$A_{1g} + A_{2u} + E_g + E_u +$ $+F_{1g} + 2F_{1u} + 2F_{2g} + F_{2u}$

Modes Classification

$$\Gamma_{\text{Raman}} = A_{1g} + E_g + 3F_{2g}$$
$$\Gamma_{\text{IR}} = 4F_{1u}$$
$$\Gamma_{\text{silent}} = A_{2u} + 2E_u + F_{1g} + 2F_{2u}$$
$$\Gamma_{\text{acoustic}} = F_{1u}$$

Polarization Selection Rules

Plane	Polarization	A_1/A_g	E/E_g	F_2/F_{2g}
(100)	XX	a^2	$4b^2$	0
(100)	$X'X'$	a^2	b^2	d^2
(100)	$X'Y'$	0	$3b^2$	0
(100)	XY	0	0	d^2
(111)	HH	a^2	b^2	d^2
(111)	HV	0	b^2	$2d^{2/3}$

to parallel and crossed polarizations of incident and scattered light.

III. LATTICE DYNAMICS CALCULATION DETAILS

Table I summarizes the results of symmetry analysis for the number, symmetry, and polarization selection rules for the Γ-point phonons in the $\alpha(P4_332)$ and $\beta(Fd\bar{3}m)$ phases of LFO. In the α phase $6A_1 + 14E + 20F_2$ phonon modes are allowed in the Raman spectra, whereas for the β phase the number of Raman allowed phonons is only five $(A_{1g} + E + 3F_{2g})$. The number of IR allowed phonons is, respectively, 21 and 4. Therefore, the α and β phases can easily be distinguished by their Raman and/or IR spectra.

We calculated the Γ-point normal modes of the α phase of $LiFe_5O_8$ by means of a shell model as implemented in the GULP package.[14] All ions in the system were assigned their nominal charges. Polarizable shells were introduced for O^{2-} and Fe^{3+} while Li^{1+} was treated as a rigid ion. The short-range interaction between ions i and j was modeled by a Born-Mayer potential: $V_{\text{BM}}(r) = A_{ij}\exp(-r/\rho_{ij}) - C_{ij}/r^6$ with van der Waals term C_{ij} retained for interactions between oxygen shells only. The parameters of the Born-Mayer potentials for the cation-anion pairs were adjusted by a fit to the crystallographic data, available for the α phase of $LiFe_5O_8$ [4] while those for the O-O interaction were taken from the data set of Lewis and Catlow.[15] The core and the shell charges X and Y, respectively, and the core-shell harmonic force constant K for O and Fe were refined in order to obtain reasonable agreement between the calculated Γ-point mode frequencies from one side and the experimental Raman (this work) and infrared-absorption [9] frequencies on the other side. Table II summarizes the adjusted model parameters. Comparison between experimental and calculated structural data for the α phase is given in Table III.

The lattice dynamics of the disordered β phase was studied in a "smeared-atom" approximation by placing at octahedral sites an average atom of mass $0.25m(\text{Li}) + 0.75m(\text{Fe})$, a

TABLE II. Shell-model parameters for the α-phase of LFO.

Atom	Core Charge X	Shell Charge Y	Core-Shell Force Constant K (eV/Å^2)
Li	+1		
Fe1/Fe2	+2	+1	598.6
O1/O2	+0.813	−2.813	75.6
Atomic Pair	A (eV)	ρ (Å)	C (eV×Å^6)
Li core–O shell	435.6	0.300	0
Fe1 shell–O shell	995.3	0.336	0
Fe2 shell–O shell	1072.9	0.336	0
O shell–O shell	22764.0	0.149	27.879

charge of +2.5, and an effective short-range interaction with oxygen shells, which is an average of the Li-O and Fe1-O potentials with the same proportions. We expect that this approximation gives a satisfactory description of the higher frequency modes involving motion of oxygen atoms mainly.

IV. RESULTS AND DISCUSSION

A. Raman spectra of α-LFO

Figure 1 shows the polarized Raman spectra of LFO-M2 obtained with 488 nm (2.54 eV) excitation with several exact scattering configurations. The spectrum at the top, where only the A_1 modes are pronounced, has been obtained by subtraction of $X'Y'$ (E) from the XX $(A_1 + E)$ spectrum. Obviously, these spectra are representative for the α phase. All A_1 Raman allowed phonons are readily identified, except the line at 616 cm^{-1} which is detectable for longer excitation wavelengths (see Fig. 4). Also 9 of 14E and 13 of 20F_2 modes are observed. It is plausible to assume that the intensity of the rest of the E and F_2 modes is below the detection limit. The frequencies of experimentally observed Raman modes are listed in Table IV along with theoretically predicted values obtained following the procedure described in Sec. II.

In contrast to normal spinels of $Fd\bar{3}m$ symmetry where Raman selection rules are quite restrictive concerning directions of atomic vibrations, in the $P4_332$ structure no simple description of the atomic displacements in Raman modes could

TABLE III. Comparison between experimental and calculated structural data of the α-phase LFO.

Parameter	Experimental	Calculated
a (Å)	8.3339	8.3342
Distances (Å)		
Fe1-O1 (×2)	2.065	2.052
Fe1-O2 (×2)	1.959	1.921
Fe1-O2 (×2)	2.015	2.000
Fe2-O1 (×1)	1.914	1.952
Fe2-O2 (×3)	1.885	1.895
Li-O2 (×6)	2.109	2.146

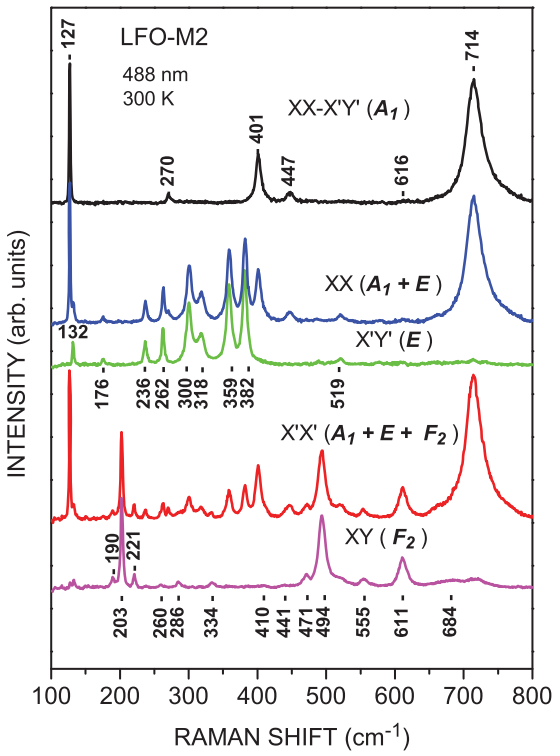

FIG. 1. (Color online) Polarized Raman spectra of $LiFe_5O_8$ (LFO-M2) obtained from (100) surface with 488 nm excitation at 300 K.

be drawn. However, in the two most intense modes of A_1 symmetry a relatively simple displacement pattern could be deduced on the basis of our calculations (see Fig. 2). The highest frequency A_1 mode at 710 cm^{-1} (experimentally 714 cm^{-1}) is similar to the A_g mode in the normal spinel structure and consists of practically uniform breathing of the FeO_4 tetrahedra while the cation sublattice is at rest. In the lowest frequency mode at 152 cm^{-1} (experimentally 128 cm^{-1}) the Fe2 and O1 atoms (both in 8c positions) move along the ⟨111⟩ set of directions, the O2 atoms follow approximately ⟨100⟩ directions, and the Fe1 atoms are displaced along ⟨110⟩. This is a "corkscrew" type of motion, being a combination of a translation along and a rotation around the Fe2-O1 bond direction of the FeO_4 tetrahedra. Lithium motion is forbidden by symmetry in all A_1 modes.

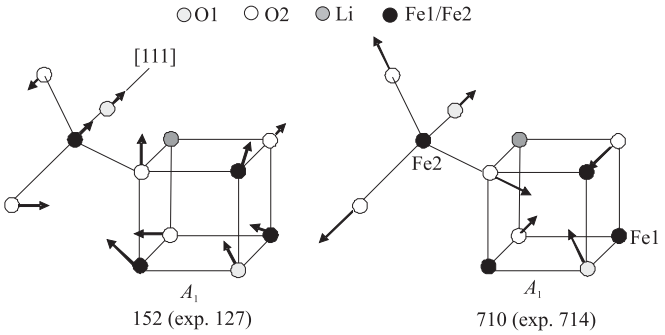

FIG. 2. Atomic displacements in the most intense A_1 normal modes of the α phase ($P4_332$) of LFO.

TABLE IV. Experimental and calculated frequencies of the Raman-active modes in $LiFe_5O_8$.

$P4_332$ Raman Modes						$Fd\bar{3}m$ Raman Modes					
A_1		E		F_2		A_{1g}		E_g		F_{2g}	
Exp.	Calc.	Exp.	Calc.	Exp.	Calc.	Exp.	Calc.	Exp.	Calc	Exp.	Calc.
127	152	132	148		147						
		176	169	190	183						
			198	203	213					201	253
		236	222	221	224						
					249						
		262	286	260	254						
270	294			286	283						
		300	312	334	309						
		318	328		385			360	286		
		359	360		392						
401	412	382	383	410	404						
447	462		407	441	456						
				471	464						
				494	500					494	476
		519	518		503						
			533	555	567						
616	595		567	611	601					609	598
			646		636						
				684	683						
714	710				715	712	697				

B. Resonance effects of α-LFO

The relative intensity of the Raman lines was found to depend significantly on the excitation photon energy. In Figs. 3 and 4 are compared, respectively, the XX and XY spectra LFO-M2 in the one- and two-phonon energy regions and extracted A_1 spectra, obtained with 633 nm (1.96 eV), 515 nm (2.41 eV), 488 nm (2.54 eV), and 458 nm (2.71 eV) excitation and normalized to the peak intensity of the 127 $cm^{-1}(A_1)$ mode. The relative intensity of the A_1 mode at 714 cm^{-1} and the two-phonon bands at 1300–1600 cm^{-1} is very low with 633 nm(1.96 eV) excitation, but strongly increases at higher photon excitation energies and even become dominant in the spectra. This observation is consistent with earlier report of a different first-order Raman spectrum of $LiFe_5O_8$ when excited with 785 nm (1.58 eV) and 515 nm (2.41 eV) laser lines.[5]

A plausible explanation for the resonant Raman scattering of $LiFe_5O_8$ can be given by noticing that another ferrite, $Bi_2Fe_4O_9$, containing both Fe^{3+}-O_4 tetrahedra and Fe^{3+}-O_6 octahedra, exhibits almost identical resonant behavior.[16] Based on the supposed electronic structure of $Bi_2Fe_4O_9$, the characteristics of its first- and second-order Raman spectra have been explained in terms of the Franck-Condon effect applied to the excitation and decay of d-d electronic excitations of the Fe^{3+} ion. In the time scale of phonon vibrations the d-d electronic transition is essentially instantaneous, which means that immediately after the transition the atomic positions are the same as in the initial state. The final state, however, requires different equilibrium positions, which is achieved by phonon emission. The Franck-Condon process manifests itself

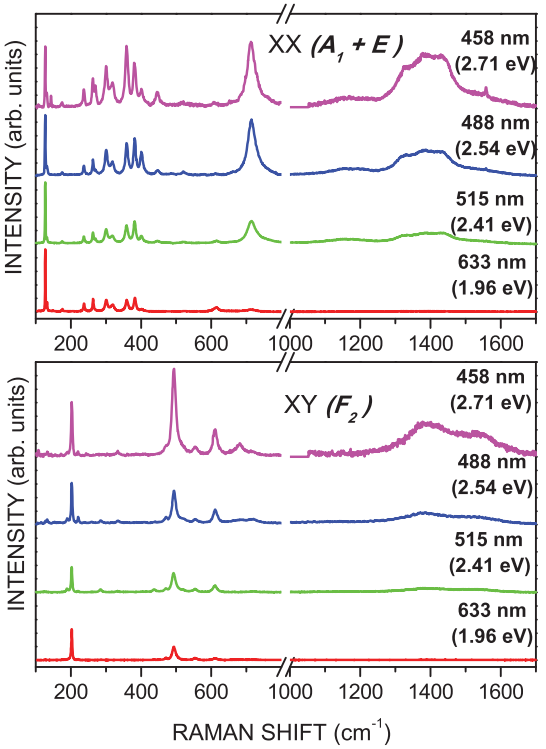

FIG. 3. (Color online) XX $(A_1 + E)$ and XY (F_2) spectra of LFO-M2 crystal obtained with various excitation photon energies at 300 K. All spectra are normalized to the peak intensity of the A_1 mode at 127 cm^{-1}.

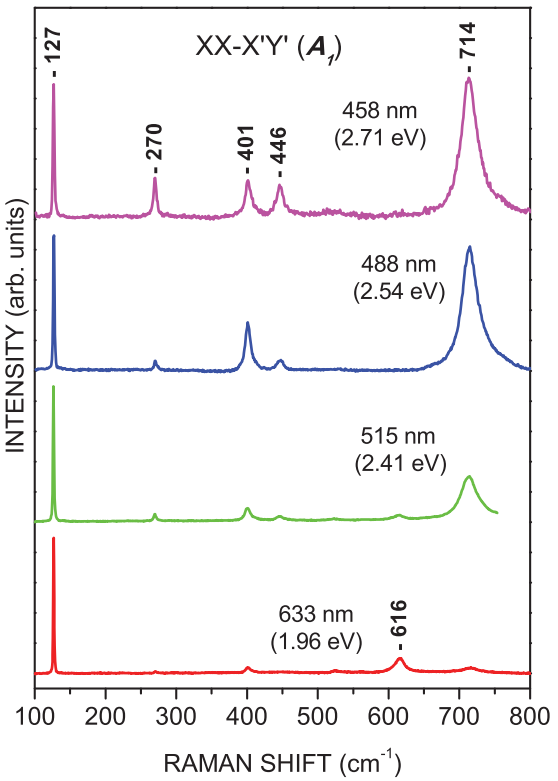

FIG. 4. (Color online) Extracted A_1 spectra LFO-M2 for various excitation photon energies. All spectra are normalized to the peak intensity of the mode at 127 cm^{-1}.

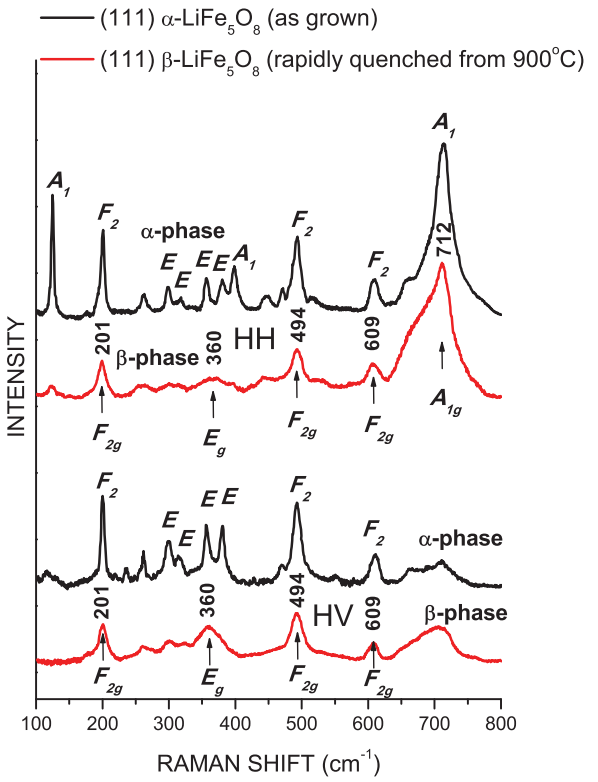

FIG. 5. (Color online) Comparison of the HH and HV spectra of α and β phases of LFO-M1 single crystal, obtained from (111) surface with 488 nm excitation at room temperature.

in enhancement of the first-order Raman bands representing the participating phonons and appearance of multiphonon bands, which replicate them. The theoretical aspects of this type of scattering have been discussed in detail by Allen and Perebeinos[17,18] on the example of $LaMnO_3$. The *d-d* transitions of Fe^{3+} in LFO in the photon energy range of interest (1.9 to 2.8 eV) are well known.[19–21] There is a weaker absorption band at 2.4 eV corresponding to transitions from the ground $^6S(A_{1g})$ to the excited $^4G(^4A_{1g},^4E_g)$ levels of $Fe^{3+}(d^5)$, split-off by the octahedral crystal field, and a stronger band at 2.56 eV, corresponding to $^6S(A_{1g}) \rightarrow ^4G(^4A_1,^4E)$ transitions in tetragonally coordinated Fe^{3+}. The photon energy of 1.96 eV (633 nm) is not sufficient to excite Fe^{3+} and thus actuate the Franck-Condon mechanism. This explains the much weaker intensity with this excitation of the A_1 (714 cm^{-1}) mode, involving in-phase vibrations of the Fe-O bonds of Fe^{3+}-O_4 tetrahedra, and the negligible intensity of the corresponding two-phonon scattering.

C. Raman spectra of β-LFO

The disordered β phase with randomly distributed Li^{1+} and Fe^{3+} at the octahedral sites has been reported to exist at either high temperatures (above 735–750 °C) or in rapidly quenched LFO samples.[3] It is not clear, however, if in the latter case the disorder is full or only partial. The reported nonpolarized Raman spectra of nominally β-LFO[6,7] are rather controversial for both, because of their inconsistency with each other and observation of a much larger number of Raman lines than expected for the $Fd\bar{3}m$ structure. More careful analysis of the spectrum reported in Ref. 6 shows that it actually corresponds to α-Fe_2O_3, the product that forms with overheating of LFO. On the other side, the β-LFO spectrum in Ref. 7 is practically identical to that of α-LFO.

We studied the α-β conversion on the example of LFO-M1 crystal, postannealed at 900 °C and rapidly quenched in liquid nitrogen. The Raman spectra obtained from the (111) plane before annealing (α phase) and after annealing and quenching (β phase) are compared in Fig. 5. The polarization selection rules for scattering from the (111) plane allow for α- and β-phase observation of the $E(E_g)$ and $F_2(F_{2g})$ phonons in both parallel (HH) and crossed (HV) scattering configurations, whereas the $A_1(A_{1g})$ phonons are allowed only in the HH spectra. The spectra of β-LFO exhibit similar resonance effects as α-LFO.

As follows from Fig. 5, the postannealing at 900 °C followed by rapid quenching results in the disappearance or strong reduction in intensity of the number of the α-phase lines, but five lines, at 201 cm^{-1}(F_{2g}), 360 cm^{-1}(E_g), 494 cm^{-1}(F_{2g}), 609 cm^{-1}(F_{2g}), and 712 cm^{-1}(A_{1g}), except for some broadening are less affected. The number and polarization properties of these lines are consistent with those expected from symmetry considerations for the β phase and can safely be assigned to it. The calculated frequencies of the three higher frequency Raman modes of the $Fd\bar{3}m$ structure correspond very well to the experimentally observed values (see the right side of Table IV), but these of the E_g mode and the lowest frequency F_{2g} mode deviate significantly from the experimental observations. This fact could be explained by the sensitivity of lower frequency vibrations to the local

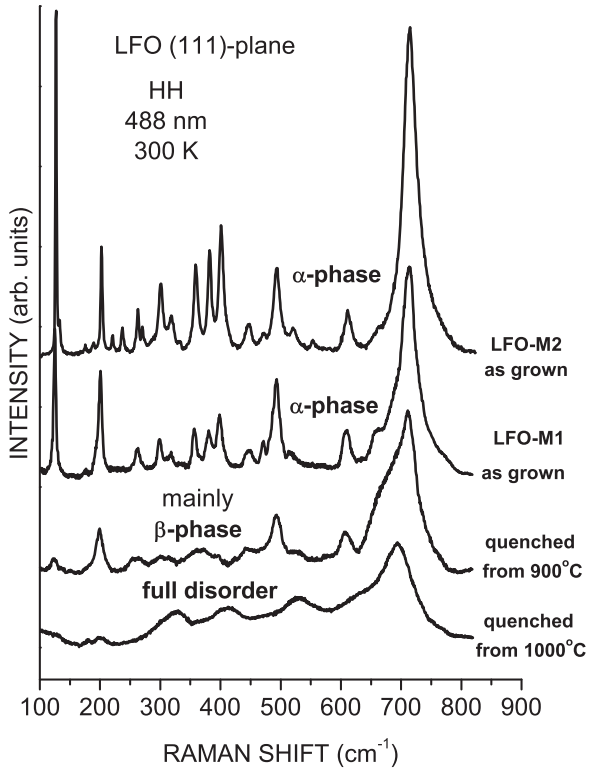

FIG. 6. HH spectra obtained from (111) surface of as-grown LFO-M1 and LFO-M2 crystals and of LFO-M1 crystals postannealed and rapidly quenched from 900 °C and 1000 °C.

atomic coordination, since according to our calculations the corresponding E mode at 360 cm^{-1} and F_2 mode at 203 cm^{-1} in $P4_332$ structure involve significant Li motion.

The observation of remnants of the α phase after several postannealings and rapid quenchings from 880 °C and 900 °C, temperatures much higher than the nominal disorder-order transition temperature, is not unexpected, as following the symmetry analysis of Haas[22] a second-order transition from a spinel crystal with 1:3 order on B sites to a disordered structure is not possible, which means that during the disordering process the system is in "mixed-phase regime" in which parts of the system have completed the transition and the other have not. The random distribution of Li^{1+} and Fe^{3+} over a long-range scale, evidenced by x-ray diffraction, not necessarily occurs at the short-range scale, where domains of ordered and disordered Li/Fe arrangement may coexist.[23] Obviously this is the case for rapidly quenched LFO after postannealing at 900 °C. The disorder, however, increases and changes its character with partial volatilization of lithium and oxygen during postannealing at temperatures 1000 °C and higher. In this case, due to significant distortions of the oxygen sublattice, its translation symmetry is lost and out-of-center phonons are activated, which results in significant spectral weight redistribution. The resulting Raman spectrum in this case represents the "smeared" phonon density of states. The difference between the Raman spectra of LFO postannealing and rapid quenching from 900 °C and 1000 °C is illustrated in Fig. 6.

V. CONCLUSIONS

We studied experimentally and theoretically the Raman spectra of the inverse spinel $LiFe_5O_8$ in its ordered α and disordered β phases and identified all observed phonons. The dependence of relative Raman intensities on the excitation phonon energy provides evidence for significant contribution of the Franck-Condon mechanism to the Raman scattering process. The B-site disordered β phase, if obtained by postannealing and rapid quenching, coexists with some amount of the ordered phase. Postannealing at higher temperatures ($\geqslant$1000 °C), however, results in significant changes of the spectra, presumably due to volatilization of Li and increasing total disorder.

ACKNOWLEDGMENTS

We thank M. Mikhov for magnetic measurements, S. Russev for EDX analysis, and B. Shivachev for help with x-ray single-crystal diffraction. This work was supported in part by the State of Texas through the Texas Center for Superconductivity at the University of Houston (TcSUH), by Grants No. TK-X-1712/2007, No. DO02-167/2008, No. DO02-56/2008, and No. DRNF 02/1 of the Bulgarian National Science Fund, as well as the Science Fund of the University of Sofia (Grant No. FNI 25/2011).

[1] A. Goldman, *Modern Ferrite Technology* (Springer, Berlin, 2006).
[2] G. O. White and C. E. Patton, J. Magn. Magn. Mater. **9**, 299 (1978).
[3] P. B. Braun, Nature (London) **170**, 1123 (1952).
[4] A. I. Smolentsev, B. Meshalkin, N. V. Podberezskaya, and B. Kaplun, J. Struct. Chem. **49**, 953 (2008).
[5] R. Aroca, M. Nazri, T. Lemma, A. Rougier, and G. A. Nazri, *Materials for Lithium-Ion Batteries*, edited by C. Julien and Z. Stoynov, NATO Science Series, Vol. 3/85 (Kluwer Academic Publishers, Dordrecht, 2000).
[6] C. M. Julien, F. Gendron, A. Amdouni, and M. Massot, Mater. Sci. Eng. B **130**, 41 (2006).
[7] W. Cook and M. Manley, J. Solid State Chem. **183**, 322 (2010).
[8] T. P. Martin, R. Merlin, D. R. Huffman, and M. Cardona, Solid State Commun. **22**, 565 (1977).
[9] E. Wolska, P. Piszora, W. Nowicki, and J. Darul, Int. J. Inorg. Mater. **3**, 503 (2001).
[10] G. M. Sheldrick, Acta Crystallogr. Sect. A **64**, 112 (2008).
[11] G. M. Sheldrick, SHELXL-97, Program for Crystal Structure Refinement, University of Göttingen, Göttingen, Germany, 1997.
[12] V. Marinova *et al.* (unpublished results).
[13] M. I. Aroyo, A. Kirov, C. Capillas, J. M. Perez-Mato, and H. Wondratschek, Acta Crystallogr. Sect. A **62**, 115 (2006).
[14] G. D. Gale, J. Chem. Soc., Faraday Trans. **93**, 629 (1997).

[15]G. V. Lewis and C. R. A. Catlow, J. Phys. C **18**, 1149 (1985).
[16]M. N. Iliev, A. P. Litvinchuk, V. G. Hadjiev, M. M. Gospodinov, V. Skumryev, and E. Ressouche, Phys. Rev. B **81**, 024302 (2010).
[17]P. B. Allen and V. Perebeinos, Phys. Rev. Lett. **83**, 4828 (1999).
[18]V. Perebeinos and P. B. Allen, Phys. Rev. B **64**, 085118 (2001).
[19]Š. Višňovský, R. Krishnan, V. Prosser, N. P. Thuy, and I. Stroda, Appl. Phys. A (Berlin) **18**, 243 (1979).
[20]V. N. Gridnev, B. B. Krichevtsov, V. V. Pavlov, and R. V. Pisarev, JETP Lett. **65**, 68 (1997).
[21]R. V. Pisarev, A. S. Moskvin, A. M. Kalashnikova, and Th. Rasing, Phys. Rev. B **79**, 235128 (2009).
[22]C. Haas, J. Phys. Chem. Solids **26**, 1225 (1965).
[23]D. H. Ridgley, H. Lessoff, and J. D. Childress, J. Am. Ceram. Soc. **53**, 304 (1970).